SINTEF
PROCEEDINGS
2

Proceedings of the 12th International Conference on Computational Fluid Dynamics in the Oil & Gas, Metallurgical and Process Industries

Progress in Applied CFD – CFD2017

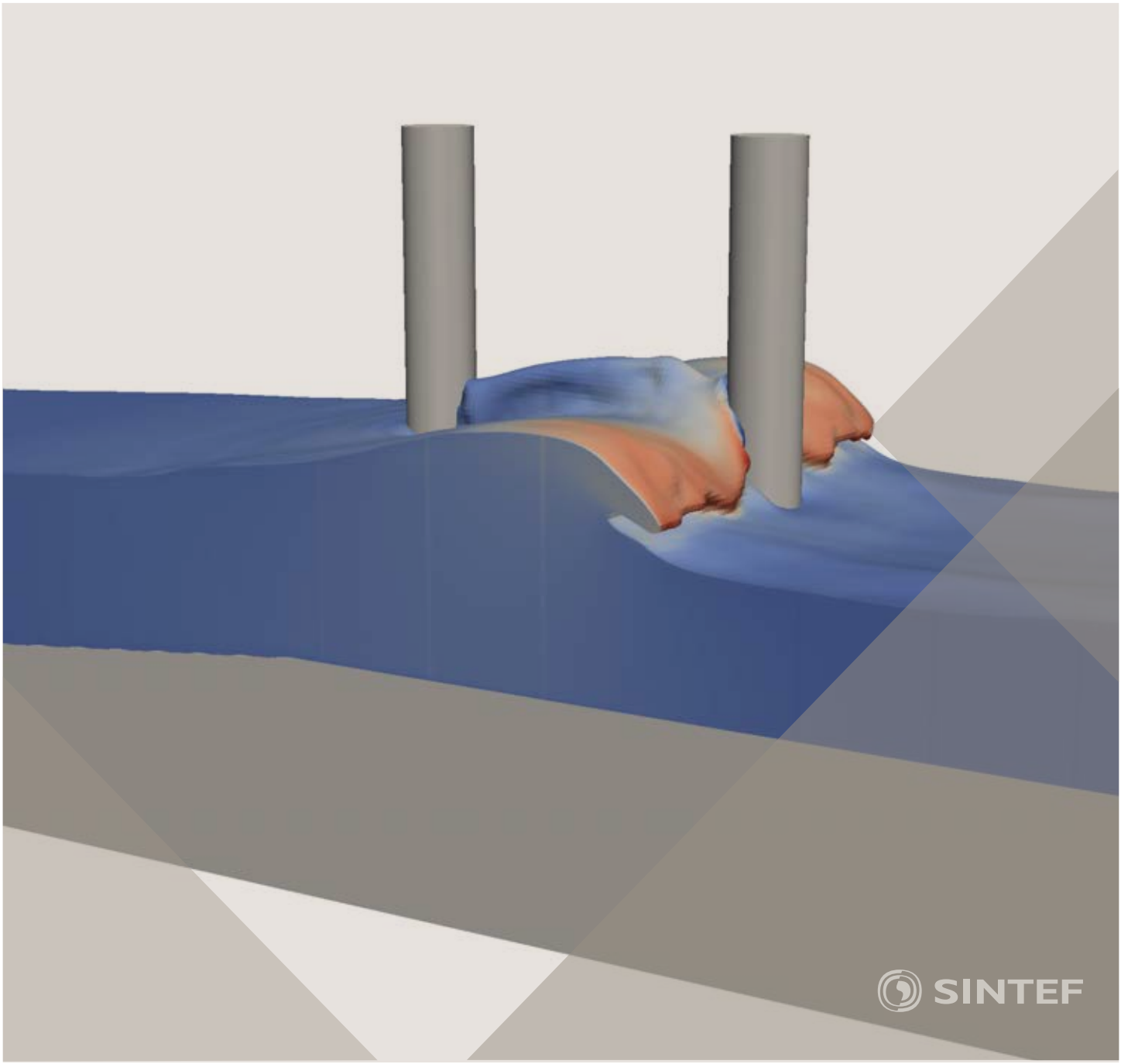

SINTEF Proceedings

Editors:
Jan Erik Olsen and Stein Tore Johansen

Progress in Applied CFD – CFD2017

Proceedings of the 12th International Conference on Computational Fluid Dynamics in the Oil & Gas, Metallurgical and Process Industries

SINTEF Academic Press

SINTEF Proceedings no 2
Editors: Jan Erik Olsen and Stein Tore Johansen
Progress in Applied CFD – CFD2017
Selected papers from 10th International Conference on Computational Fluid Dynamics in the Oil & Gas, Metallurgical and Process Industries

Key words:
CFD, Flow, Modelling

Cover, illustration: Arun Kamath

ISSN 2387-4295 (online)
ISBN 978-82-536-1544-8 (pdf)

SINTEF Academic Press
Address: Forskningsveien 3 B
PO Box 124 Blindern
N-0314 OSLO
Tel: +47 73 59 30 00
Fax: +47 22 96 55 08

www.sintef.no/byggforsk
www.sintefbok.no

SINTEF Proceedings
SINTEF Proceedings is a serial publication for peer-reviewed conference proceedings on a variety of scientific topics.
The processes of peer-reviewing of papers published in SINTEF Proceedings are administered by the conference organizers and proceedings editors. Detailed procedures will vary according to custom and practice in each scientific community.

PREFACE

This book contains all manuscripts approved by the reviewers and the organizing committee of the 12th International Conference on Computational Fluid Dynamics in the Oil & Gas, Metallurgical and Process Industries. The conference was hosted by SINTEF in Trondheim in May/June 2017 and is also known as CFD2017 for short. The conference series was initiated by CSIRO and Phil Schwarz in 1997. So far the conference has been alternating between CSIRO in Melbourne and SINTEF in Trondheim. The conferences focuses on the application of CFD in the oil and gas industries, metal production, mineral processing, power generation, chemicals and other process industries. In addition pragmatic modelling concepts and bio-mechanical applications have become an important part of the conference. The papers in this book demonstrate the current progress in applied CFD.

The conference papers undergo a review process involving two experts. Only papers accepted by the reviewers are included in the proceedings. 108 contributions were presented at the conference together with six keynote presentations. A majority of these contributions are presented by their manuscript in this collection (a few were granted to present without an accompanying manuscript).

The organizing committee would like to thank everyone who has helped with review of manuscripts, all those who helped to promote the conference and all authors who have submitted scientific contributions. We are also grateful for the support from the conference sponsors: ANSYS, SFI Metal Production and NanoSim.

Stein Tore Johansen & Jan Erik Olsen

Organizing committee:

Conference chairman: Prof. Stein Tore Johansen
Conference coordinator: Dr. Jan Erik Olsen
Dr. Bernhard Müller
Dr.Sigrid Karstad Dahl
Dr.Shahriar Amini
Dr.Ernst Meese
Dr.Josip Zoric
Dr.Jannike Solsvik
Dr.Peter Witt

Scientific committee:

Stein Tore Johansen, SINTEF/NTNU
Bernhard Müller, NTNU
Phil Schwarz, CSIRO
Akio Tomiyama, Kobe University
Hans Kuipers, Eindhoven University of Technology
Jinghai Li, Chinese Academy of Science
Markus Braun, Ansys
Simon Lo, CD-adapco
Patrick Segers, Universiteit Gent
Jiyuan Tu, RMIT
Jos Derksen, University of Aberdeen
Dmitry Eskin, Schlumberger-Doll Research
Pär Jönsson, KTH
Stefan Pirker, Johannes Kepler University
Josip Zoric, SINTEF

CONTENTS

EXPERIMENTAL AND NUMERICAL STUDY ON SINGLE DROPLET BREAKAGE IN TURBULENT FLOW

Jing SHI*, Eirik Helno HERØ, Jannike SOLSVIK, Hugo Atle JAKOBSEN*

NTNU Department of Chemical Engineering, 7491 Trondheim, NORWAY

* Correspondence concerning this article should be addressed to J. Shi at Jingshi1988@gmail.com or H. A. Jakobsen at hugo.a.jakobsen@ntnu.no

ABSTRACT

Droplet size distributions in liquid-liquid turbulent flow are determined by droplet breakage and coalescence. The current understanding of these processes are not sufficient. An experimental study on single droplet breakage in turbulent flow, where coalescence can be neglected, is presented in this paper to study the droplet breakage mechanism. A rectangular channel consisting of a pair of opposite steel walls having a series of stationary protuberances to enhance turbulence level, and a pair of opposite glass walls that are smooth to facilitate image capture of the droplet breakage process is used as the droplet breakage channel. The commercial CFD code FLUENT is utilised to simulate the continuous single-phase flow in the droplet breakage channel with interest particularly in the turbulent characteristics such as the turbulent kinetic energy and turbulent energy dissipation rate, as these parameters are closely related to the droplet breakage process. The large eddy simulation (LES) method was used to provide detailed features of the flow. Results from LES were also compared with those from a RANS model (SST k-ω). The simulation results demonstrated that the turbulence level is enhanced across the pair of walls with protuberances. There are more coherent strong vortices in the region close to the wall with protuberances. Some preliminary experimental results on droplet breakage are also presented.

Keywords: Breakage, large eddy simulation (LES), turbulent energy dissipation rate, turbulent vortical structures.

NOMENCLATURE

Greek Symbols

ϵ Turbulent energy dissipation rate, [m^2/s^3].
$\langle\epsilon\rangle$ Time averaged turbulent energy dissipation rate, [m^2/s^3].
κ von Kármán constant, 0.4187, [-].
ν Molecular kinematic viscosity, [m^2/s].
ν_{SGS} Subgrid eddy viscosity, [m^2/s].
ξ Length scale, [m].
τ_{ij}^{SGS} Subgrid stress tensor, [m^2/s^2].
$\bar{\omega}_{ij}$ Vorticity tensor, $\bar{\omega}_{ij} = \frac{1}{2}\left(\frac{\partial \bar{u}_i}{\partial x_j} - \frac{\partial \bar{u}_j}{\partial x_i}\right)$, [1/s].
Δ Filter width, [m].
$\mathbf{\Omega}$ Absolute value of vorticity, $\mathbf{\Omega} = \sqrt{2\bar{\omega}_{ij}\bar{\omega}_{ij}}$, [1/s].

Latin Symbols

C_s Smagorinsky constant, 0.1, [-].
d Distance to the closest wall, [m].
G Filter function, [1/m].
$\langle\bar{k}\rangle$ Time averaged turbulent kinetic energy, [m^2/s^2].
L_S Mixing length for the subgrid scale, [m].
$\bar{p}$ Pressure, [Pa].
Q Criterion for illustrating coherent vortexes, [1/s^2].
$\bar{S}_{ij}$ Rate of strain tensor, $\bar{S}_{ij} = \frac{1}{2}\left(\frac{\partial \bar{u}_i}{\partial x_j} + \frac{\partial \bar{u}_j}{\partial x_i}\right)$, [1/s].
$\mathbf{S}$ Absolute value of the strain rate, $\mathbf{S} = \sqrt{2\bar{S}_{ij}\bar{S}_{ij}}$, [1/s].
t Time scale, [s].
u_i Velocity, [m/s].
$\bar{u}$ Filtered/resolved velocity in LES, [m/s].
u_i' Filtered residual velocity in LES, [m/s].
$\langle\bar{u}_i\rangle$ Time averaged velocity, [m/s].
$\bar{V}$ Mean velocity (experiments), [m/s].
V_k Volume of a computational cell, [m^3].
x Length scale, [m].

Sub/superscripts

i Index *i*.
j Index *j*.
k Index *k*.

INTRODUCTION

Dispersed liquid-liquid systems are quite common in different industries, for example, the chemical, pharmaceutical, food, and petroleum industries. The fluid particle size is determined by equilibrium between various mechanisms of fluid particle breakage and coalescence. Most of the engineering flow problems are turbulent in nature. Many of the existing models that describe particle breakup in turbulent flow are based on the work of Coulaloglou and Tavlarides (1977). It is assumed that the droplets are in a turbulent flow field which is locally isotropic and the droplet size is within the inertial subrange. The authors proposed a premise that a drop would break if the turbulent kinetic energy transmitted to the drop from the turbulent eddies exceeds the drop surface energy and only eddies smaller than the particle diameter may transmit the energy. Reviews on the different models of particle breakage can be found in Lasheras et al. (2002), Liao and Lucas (2009) and Solsvik et al. (2013). The aforementioned reviews show that the predictions from different breakage models can be contradictory. Many of the models are derived from

assumptions that have not been validated experimentally. There is little reliable experimental data in the literature that can be used to validate different models. Therefore, it is of importance to experimentally investigate the breakage process and further obtain reliable data for model evaluation.

Many experimental studies on droplet breakage investigated the properties of final particle population, such as the maximum stable particle size, mean particle size and the particle size distribution as a function of the mean particle size (e.g., Sleicher, 1962; Sprow, 1967; Middleman, 1974; Calabrese et al., 1986; Wang and Calabrese, 1986; Angeli and Hewitt, 2000a; Azizi and Al Taweel, 2011). Experiments on single droplet breakage in turbulent flow, where coalescence can be neglected, have been undertaken by researchers more recently. Andersson and Andersson (2006) studied both bubble and droplet breakup in flow of immiscible fluids through a static mixer or channel reactor. The turbulence generated in this channel reactor in general is more homogeneous compared to a stirred tank reactor as turbulence is continuously produced and dissipated along the reactor. The experimental results from the above authors demonstrated differences in the bubble breakup and droplet breakup. The bubble breakup mainly resulted in two fragments while multiple breakup was more frequently observed in droplet breakup. Also, the bubble breakup often resulted in unequal size fragments while fragments upon droplet breakup had a higher probability of being approximately equal size than unequal size. Maaß et al. (2007) and Maaß and Kraume (2012) investigated single droplet breakage in turbulent flow in a breakage cell which was designed to reflect the flow field in the impeller region of a stirred tank. The breakage cell was a rectangular channel with a single blade representative of a section of a Rushton turbine inserted into the channel from one side. The results showed that the highest probability with regard to the number of fragments formed upon breakup was for the binary breakup. The average breakage time appeared to have a minimum for a certain mother drop diameter. The relative numbers of distributions of the breakage time were best fit with a β-distribution instead of normal distribution. Solsvik and Jakobsen (2015) experimentally investigated single droplet breakup in a stirred tank. It was reported that multiple breakup events (specifically, more than 2 daughter drops, and up to more than 9 fragments) were more frequently observed than binary breakup. Also, unequal-sized rather than equal-sized breakup was more frequently observed. For all of the aforementioned experimental studies on single droplet breakage, the high-speed imaging technique was applied to capture the breakage process. The statistical information on breakage process is obtained by further image processing. Detailed information which is of great value for evaluating the breakage models, e.g., the statistical distributions of breakage time, breakage probability, daughter numbers and sizes, can be obtained by experiments on single droplet breakage.

In addition to statistical information on droplet breakage, information of the underlying turbulent parameters, particularly the local turbulent energy dissipation rate, ε, is desirable. The local turbulent energy dissipation rate is one of the variables in most of the breakage models. As the local turbulent energy dissipation rate is usually not known, the average energy dissipation rate is used instead in many studies. Experimental measurement of the turbulent energy dissipation rate can be achieved by the particle image velocimetry (PIV) technique. However, the estimation of the turbulent energy dissipation rate from the PIV measurements is not straightforward and require careful evaluation (Jong et al., 2009). Since CFD has become a standard tool for flow prediction, the single-phase simulation could provide some useful information on the turbulent parameters. Bouaifi et al. (2004) conducted both PIV measurements and CFD simulation of the flow in a channel reactor which is the experimental system used in the particle breakage study reported in Andersson and Andersson (2006). Several different k-ε models implemented in FLUENT were used in their CFD simulation. The turbulent parameters from the CFD simulations were comparable to those estimated from PIV measurements. Maaß et al. (2007) also used the k-ε models to simulate the flow field of a breakage cell. The k-ε models are practical turbulent models based on solving Reynolds Averaged Navier-Stokes Equations (RANS) together with the turbulence closures. The two-equation turbulent models (e.g., k-ε models, k-ω models) inherently apply an assumption of isotropic turbulent viscosity thus there could be large uncertainties in the CFD predictions of the flow where highly anisotropic turbulence exists. Another attractive method is Large Eddy Simulation (LES). In LES the Navier–Stokes equations are spatially filtered, which eliminates eddies whose scales are smaller than a filter width. Large eddies are directly resolved, while small eddies are modelled using subgrid scale models that describe the interactions between the large eddies and the unresolved smaller scales. LES results are theoretically more comparable to PIV measurements as the experimental data obtained by PIV are similar to the filtering method used in LES (Sheng et al., 2000). Ni et al. (2003) applied both LES and PIV to quantify turbulent properties in an oscillatory baffled column. The authors reported good agreement between these two techniques. Delafosse et al. (2008) performed simulations of flow in a stirred tank using both the standard k-ε model and the LES model and compared the simulation results with PIV measurements. It was demonstrated that the LES gave better predictions in the turbulent parameters.

The aim of this study is to carry out an experimental campaign on single droplet breakage in turbulent flow to obtain the statistical information of the breakage process, and to perform CFD simulation of the single-phase flow using the LES method to have a picture of the underlying turbulent parameters related to droplet breakage. Results from the LES simulation were also compared with those from a steady RANS model (SST k-ω). In this paper, the experimental setup is first introduced followed by introduction of the CFD models and simulation setup. In the following section on results, some preliminary experimental results are presented first, followed by the CFD results. Finally, the conclusions and some future work are presented.

EXPERIMENTAL SETUP

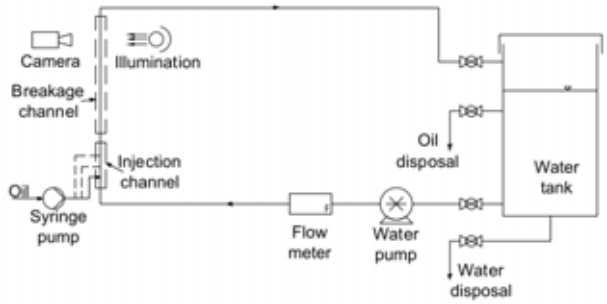

Figure 1: Schematic diagram of the experimental setup.

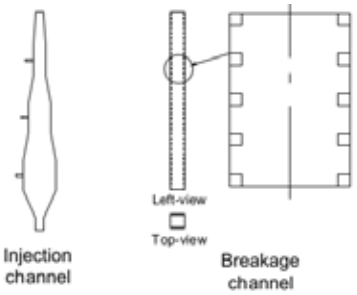

Figure 2: Schematic diagram of the injection channel (a) and the breakage channel (b).

The experimental setup used in this study is depicted in Figure 1. The de-ionized water is stored in a tank (capacity: 1 m^3) and pumped by a positive displacement pump (PDP). The water flow is metered using an electromagnetic meter (SIEMENS SITRANS F M MAG 5100 W, DN 25). The water flows through a vertical pipeline which is the major part of the flow loop. The vertical line consists of two sections – the injection channel and the breakage channel. Dyed-oil pumped by a syringe pump is injected into the pipeline at the injection channel upstream of the vertical pipeline. This section is made from transparent glass and composed of three rectangular channels of different cross-sectional areas and the channels with varying cross-sections which smoothly connect the rectangular channels (see Figure 2 (a)). At a constant water flow rate in the flow loop, the size of the injected oil drop varies when injected via the different injection ports. Downstream of the injection channel is the breakage channel where the droplet breakage in turbulent water is investigated. This section is a rectangular channel (30×30×1000 mm^3) consisting of a pair of opposite steel walls which have a series of stationary protuberances/tabs to enhance turbulence level, and a pair of opposite glass walls that are smooth to facilitate image capture of the droplet breakage process (see Figure 2 (b)). High-speed cameras (Photron FASTCAM Mini AX100) are used to record the breakage process of an oil droplet in turbulent flow with a frame rate of at least 4000 fps.

After the vertical pipeline, the fluids flow back to the water tank. Here the water tank also serves as a separator as the tank capacity is quite large and contains a large volume of water while the amount of oil used in experiments is very small compared to that of the water. The water in the lower part of the tank can be kept uncontaminated from oil thus cyclic operation can be realised. The tank has a viewing window to allow for liquid level monitoring. Disposal of oil should be carried out when the purity of the water in the lower part of the tank would be affected with increased heights of the oil layer and the emulsion layer after some time of experiments with accumulation of oil droplets.

NUMERICAL SIMULAITON

Governing Equations

The governing equations for LES are obtained by spatially filtering over small scales. A generalized filter can be defined by

$$\bar{u}_i(x,t) = \iiint G(x-\xi;\Delta)u_i(\xi,t)d^3\xi \qquad (1)$$

where the filter function is interpreted as acting to keep values of u_i occurring on scales larger than the filter width Δ. G is some function that is effectively zero for values of u_i occurring at the small scales. By filtering the Navier–Stokes equations, the velocity field has the decomposition

$$u_i(x,t) = \bar{u}_i(x,t) + u_i'(x,t) \qquad (2)$$

By filtering the Navier–Stokes equations, the governing equations employed for LES are obtained as

$$\frac{\partial \bar{u}_i}{\partial x_i} = 0 \qquad (3)$$

$$\frac{\partial \bar{u}_i}{\partial t} + \frac{\partial \bar{u}_i\bar{u}_j}{\partial x_j} = -\frac{1}{\rho}\frac{\partial \bar{p}}{\partial x_i} + \frac{\partial}{\partial x_j}\left(\nu\frac{\partial \bar{u}_i}{\partial x_j}\right) - \frac{\partial \tau_{ij}^{SGS}}{\partial x_j} \qquad (4)$$

where $\tau_{ij}^{SGS} = \overline{u_iu_j} - \bar{u}_i\bar{u}_j$. The subgrid stress tensor τ_{ij}^{SGS} describes the transfer of momentum by turbulence at scales that are smaller than the filter. The subgrid-scale stresses are unknown and require modelling. In this study, one frequently used subgrid model in the literature, namely, Smagorinski-Lily model, is used. The unresolved stresses follows

$$\tau_{ij}^{SGS} - \frac{1}{3}\tau_{kk}^{SGS}\delta_{ij} = -2\nu_{SGS}\bar{S}_{ij} \qquad (5)$$

$$\nu_{SGS} = L_s^2|\bar{s}| = L_s^2\sqrt{2\bar{S}_{ij}\bar{S}_{ij}} \qquad (6)$$

where $\bar{S}_{ij}$ is the rate of strain tensor for the resolved scale, $\bar{S}_{ij} = \frac{1}{2}\left(\frac{\partial \bar{u}_i}{\partial x_j} + \frac{\partial \bar{u}_j}{\partial x_i}\right)$; ν_{SGS} is the subgrid eddy viscosity; and L_S the mixing length for the subgrid scale, $L_S = \min(\kappa d, C_s V_k^{1/3})$, in which κ denotes the von Kármán constant, 0.4187, d the distance to the closest wall, V_k the volume of a computational cell, and C_s the Smagorinsky constant. The default value in FLUENT, $C_s = 0.1$, was used in this study.

Simulation Setup

The commercial CFD package FLUENT was used for the simulation. The simulation geometry is depicted in Figure 3 (a). The geometry resembles a short section of the experimental breakage channel along the flow direction, which is 60mm along Y-axis. Figure 3 (b) illustrates the mesh of the cross-section marked in Figure 3 (a). To satisfy the mesh requirement for LES simulation and to capture sufficiently detailed flow structures, the mesh (hexahedral cells) is very fine in general and is progressively finer near the walls (the lengths of cells ranged between 0.02-0.6 mm). The total number of cells

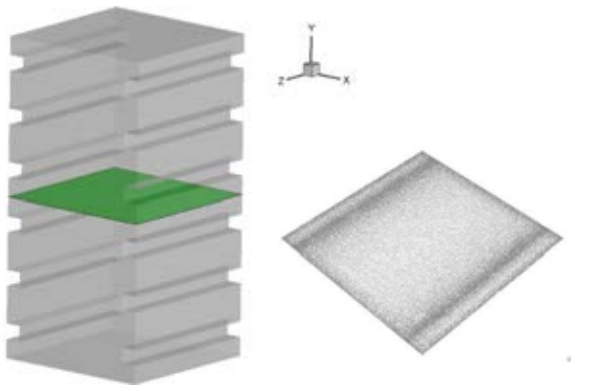

(a) (b)

Figure 3: The simulation geometry (a) and mesh of a cross-section (b).

is about 7.4 million. The wall y+ for a flow rate of 2 m/s ranged between 0.01 and 5.9 with the majority of the cells having y+ between 0.01 and 3.

The fluid in this study was water (density: 998.2 kg/m^3, viscosity: 1.003 mPa.s). The periodic flow boundary was applied to model the developed flow in the channel. The mass flow rate was specified (0.9 and 1.8 kg/s, corresponding average velocities of 1 and 2 m/s, respectively). A steady RANS simulation with the k-ω SST model was first run before the LES simulation. The solutions from the RANS simulation were used as the initial conditions of the LES simulation.

The pressure-velocity coupling algorithm was used to solve the transport equations. The PRESTO! (pressure staggering option) scheme was used for the pressure interpolation. The SIMPLE (semi-implicit method for pressure linked equations) scheme was used for the pressure-velocity coupling. The bounded central differencing discretization scheme for momentum equations was applied. The bounded second order implicit scheme was used for the transient formulation. The time step used was 2×10^{-5} s. The pressure gradient was monitored as well as the residuals of the transport equations for the judgement of convergence. Convergence was regarded to be achieved when the monitored values are statically stable (that is after at least 3 flow-through time). The converged pressure gradients were close to theoretical predictions of developed channel flow for corresponding mass flow rates, thus the calculations were regarded as reasonable.

As the LES solves an approximately instantaneous velocity field, post-processing is needed to obtain the turbulent parameters of interest. This can be achieved by defining custom field functions and sampling the data in Fluent. The following definitions were applied to estimate ensemble/time averaged turbulent kinetic energy and dissipation rate (Ni et al., 2003; Delafosse et al., 2008).

Turbulent kinetic energy:

$$\langle \bar{k} \rangle = \frac{1}{2}\left(\frac{\sum_{n=1}^{N} \overline{u_\iota}\,\overline{u_\iota}}{N} - \langle \overline{u_\iota} \rangle^2\right) \quad (7)$$

$$\langle \overline{u_\iota} \rangle = \frac{1}{N}\sum_{n=1}^{N} \overline{u_\iota} \quad (8)$$

Turbulent energy dissipation rate:

$$\langle \epsilon \rangle = \frac{1}{N}\sum_{n=1}^{N} \epsilon \quad (9)$$

$$\epsilon = 2(\nu_{SGS} + \nu)\bar{S}_{ij}\bar{S}_{ij} \quad (10)$$

where $\langle \bar{k} \rangle$ denotes ensemble/time averaged turbulent kinetic energy over N samples, $\overline{u_\iota}$ resolved velocity, and $\langle \overline{u_\iota} \rangle$ ensemble/time averaged velocity over N samples. $\langle \epsilon \rangle$ denotes ensemble/time averaged turbulent energy dissipation rate over N samples, ν_{SGS} the subgrid kinematic eddy viscosity, ν molecular kinematic viscosity, and $\bar{S}_{ij}$ rate-of-strain tensor for the resolved scale.

With definitions of parameters of interest via custom field functions, data sampling was performed at a time interval of 4×10^{-5} s for at least 2 flow-through time, obtaining samples of a number of over 1000. With 64 parallel processors of 4 nodes from a cluster, the CPU time used was around 96h for a typical run.

RESULTS

Preliminary Experimental Results

Some preliminary tests were conducted using the food oil (olive oil). The approximate viscosity of the oil is 80 mPa.s. The interfacial tension between the un-dyed oil and water is around 16.4 mN/m. It is noted that the interfacial tension can be affected by the addition of the dye (Sudan Black B). The interfacial tensions between the dyed oils and water would be measured in the future.

Figure 4 illustrates the deformation process of a single droplet. The flow rate of the continuous flow is 1 m/s for this case. In this case, the droplet was slightly deformed in the central region of the channel, and it endured further deformation when it migrated into the region closer to the wall with protuberances. The highly deformed drop appeared dumbbell-shaped before it went out of the view area. To realize tracking the breakage process as complete as possible and at the same time obtaining high-speed photographs with sufficient spatial resolution, synchronized multiple high-speed cameras positioned along the flow direction will be applied in the future.

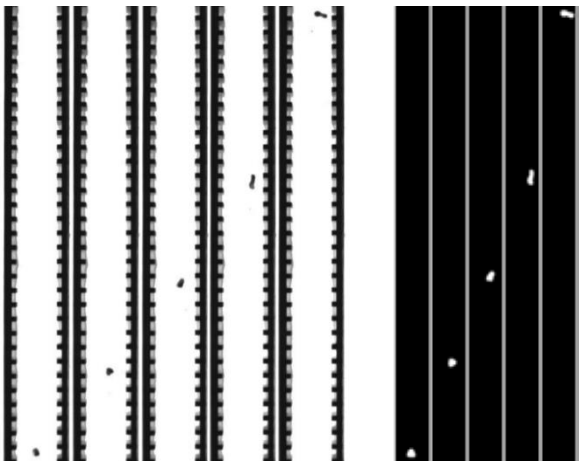

(a) (b)

Figure 4: Illustration of the deformation process of a droplet. (a) High-speed images (b) Images after processing.

CFD Results

Velocity Field

The resolved velocity field from LES at one instant, which is approximately the instantaneous velocity field, is illustrated in Figure 5. It is demonstrated that there are backflow vortices below each protuberance/tab. The influence of the tabs on the pair of opposite walls is mainly 2-dimensional, with the flow field across the z-axis similar to that of a channel with smooth walls.

The profiles of the Y velocity (velocity component in the flow direction) along the lines of symmetry of a cross-section of the channel are described in Figure 6. In addition to the results from LES, the resolved velocities from the steady RANS simulation (SST k-ω), which were in fact the initial conditions of the LES, are also depicted in Figure 6. The size of the protuberances is indicated by the dash lines in Figure 6 (b) as well as following relevant figures. In general, a good agreement is shown between the mean velocities from the LES and RANS simulation. However, it was shown from Figure 6 (b) that the highest backflow magnitude from the RANS simulation is slightly lower than that from LES. Also, the velocity profile from RANS is flatter across the central region of the channel.

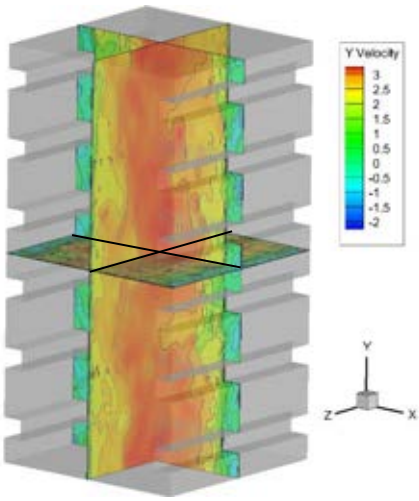

Figure 5: Contours of the resolved velocity (approximately the instantaneous velocity) at one instant from LES ($\bar{V} = 2m/s$).

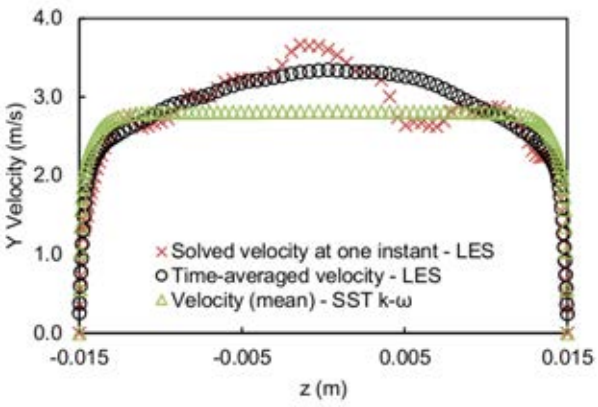

(a)

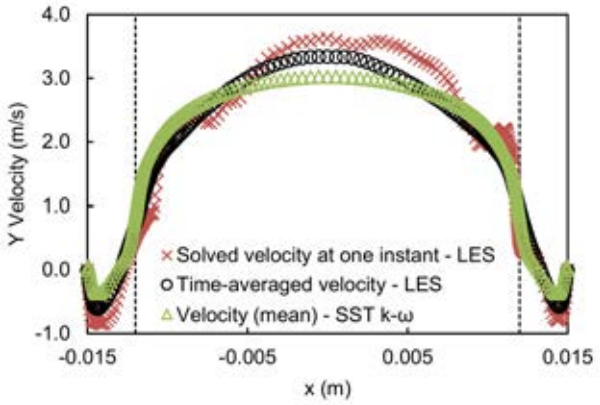

(b)

Figure 6: Y velocity along the lines of symmetry of a cross-section of the channel from LES and SST k-ω turbulence model ($\bar{V} = 2m/s$). (a) Across the pair of smooth walls; (b) Across the pair of walls with tabs.

Turbulent Kinetic Energy

The profiles of turbulent kinetic energy (TKE) along lines of symmetry of a cross-section of the channel are described in Figure 7. The TKE from LES illustrated are the ensemble/time averaged values calculated following Equations (7-8). The general trends of TKE from the LES and RANS simulation are consistent. However, the TKE from the LES is in general higher than that from the SST k-ω model. Similar magnitudes of TKE are shown in the central region of the channel, while the highest TKE locating close to walls/tabs from the LES is about one time higher than that from the SST k-ω turbulence model.

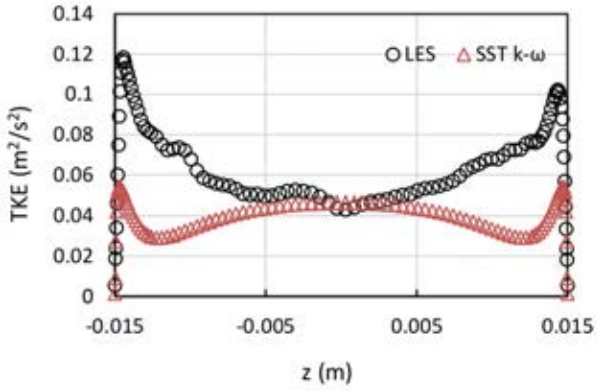

(a)

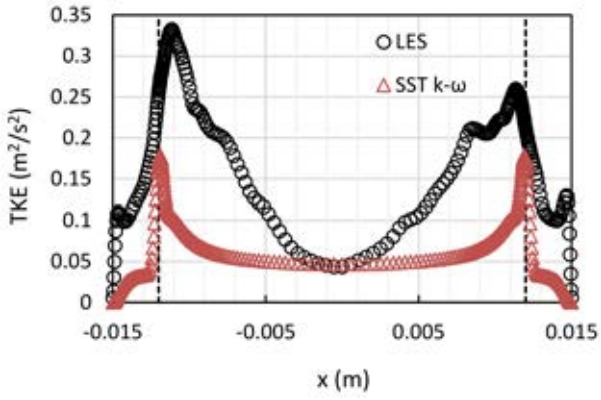

(b)

Figure 7: Turbulent kinetic energy along the lines of symmetry of a cross-section of the channel from LES and SST k-ω turbulence model ($\bar{V} = 2m/s$). (a) Across the pair of smooth walls; (b) Across the pair of walls with tabs.

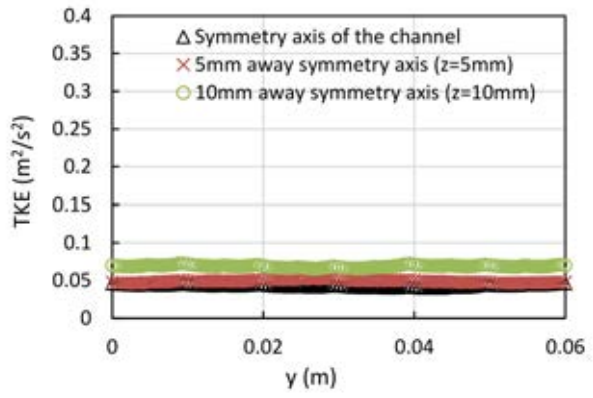

(a)

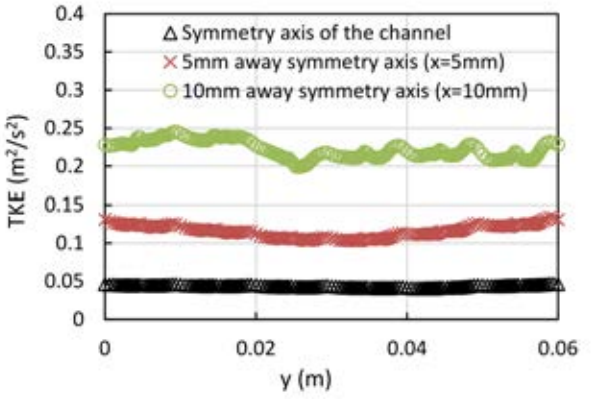

(b)

Figure 8: Turbulent kinetic energy from LES ($\bar{V} = 2m/s$) along different lines parallel to the symmetry axis of the channel in symmetry planes of the channel**.** (a) In the symmetry plane across the pair of smooth walls; (b) In the symmetry plane across the pair of walls with tabs.

The SST k-ω model inherently applies an assumption of isotropic turbulent viscosity thus there could be large uncertainties in the CFD predictions of the flow close to walls where highly anisotropic turbulence exists. The TKE from the LES shows less homogeneity in the central region of the channel than that from the SST k-ω model in Figure 7 (b). Comparing Figure 7 (b) to Figure 7 (a), it is shown that the turbulence kinetic energy is increased across the pair of walls with tabs, which fits the purpose of increasing the turbulence level hence enhancing the occurrence of droplet breakage by using a pair of walls with increased roughness. The profiles of the turbulent kinetic energy along different lines parallel to the symmetry axis of the channel in symmetry planes of the channel are depicted in Figure 8. As have been demonstrated by Figure 7, Figure 8 in another way shows that the turbulence kinetic energy is increased across the pair of walls with tabs.

Turbulent Energy Dissipation Rate

The profiles of turbulent energy dissipation rate (TDR) along lines of symmetry of a cross-section of the channel are described in Figure 9. The general trends of TDR from the LES and the SST k-ω model are consistent along the z direction, i.e., across the pair of smooth walls, as shown in Figure 9 (a). The magnitudes of TDR in the central region of the channel along the z direction from the LES and the SST k-ω model are close. The LES

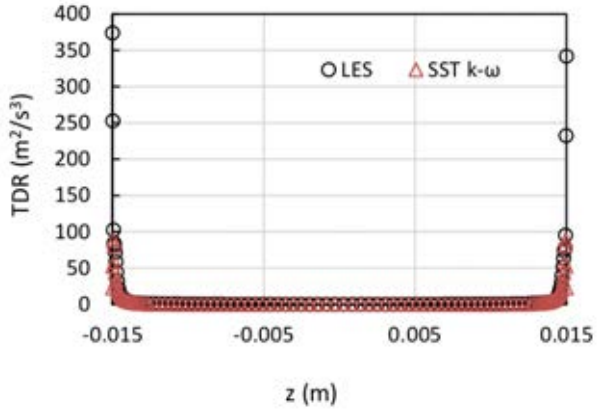

(a)

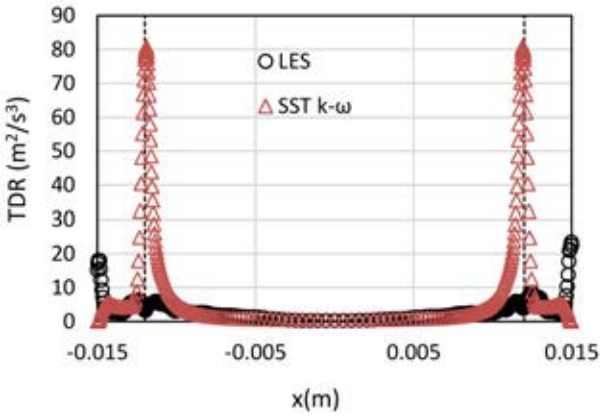

(b)

Figure 9: Turbulent energy dissipation rate along the lines of symmetry of a cross-section of the channel from LES and SST k-ω turbulence model ($\bar{V} = 2m/s$). (a) Across the pair of smooth walls; (b) Across the pair of walls with tabs.

predicts higher TDR in the near-wall region than the SST k-ω model. Some inconsistence is demonstrated in the general trends of TDR from the LES and the SST k-ω model along the x direction, i.e., across the pair of walls with tabs, as shown in Figure 9 (b). The predicted TDR across the pair of walls with tabs from LES has its highest value in the near-wall region, endures a decrease before it increases as approaching the region behind the tap wall (the tab wall is in alinement with x=±0.012 m); it gradually decreases again as approaching to the central region of the channel. The predicted TDR across the pair of walls with tabs from the SST k-ω turbulence model is very low in the near-wall region, endures a gradual increase first then a sharp increase to its peak as approaching the region behind the tap wall. It decreases sharply as passing the region behind the tap wall. It is difficult to explain the different trends as the methods from which the turbulent energy dissipation rate are calculated TDR from LES are calculated following Equations (9-10). The accuracy of the TDR from LES can be affected by the mesh scales and the subgrid-scale model. The k-equation and ω-equation of the SST k-ω turbulence model serve as empirical closures to solve the Reynolds Averaged Navier-Stokes Equations. The k-equation is directly deduced from Reynolds Averaged Navier–Stokes equations, denoting an exact equation for the turbulent kinetic energy. The greatest amount of uncertainty and controversy usually lies in the ω-equation which is not directly derived from an exact equation (Wilcox, 1988). Also, as an assumption of

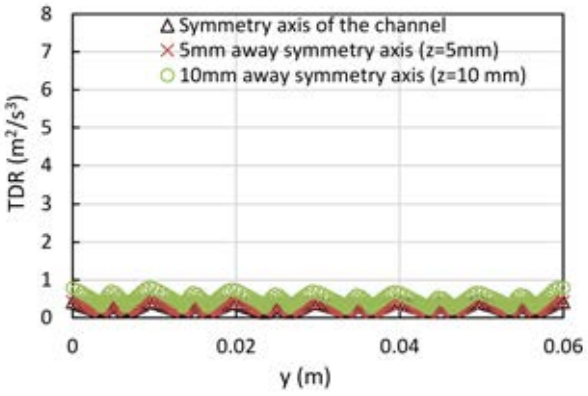

(a)

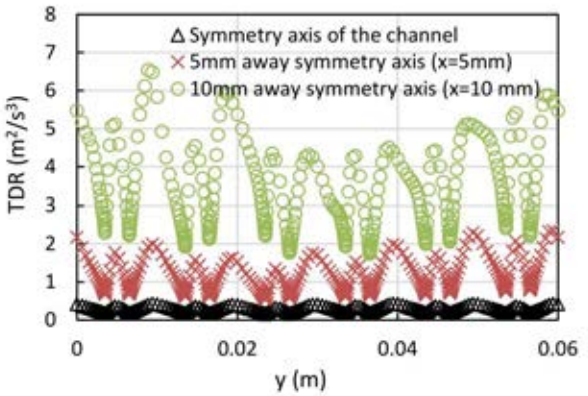

(b)

Figure 10: Turbulent energy dissipation rate from LES ($\bar{V} = 2m/s$) along different lines parallel to the symmetry axis of the channel in symmetry planes of the channel**.** (a) In the symmetry plane across the pair of smooth walls; (b) In the symmetry plane across the pair of walls with tabs.

isotropic turbulent viscosity is used in RANS simulation, there could be large uncertainties in the CFD predictions of the flow behind the taps where highly anisotropic turbulence exists.

It is difficult to see whether the turbulent energy dissipation rate in the central region of the channel is increased or not across the wall with tabs from Figure 9 as the scale range is quite large. The profiles of the turbulent energy dissipation rate along different lines parallel to the symmetry axis of the channel in symmetry planes of the channel are depicted in Figure 10. Comparing Figure 10 (a) and (b), it is demonstrated that the turbulent energy dissipation rate in the central region of the channel is increased across the wall with tabs. Also, it shows that the turbulence in the central region of the channel is less homogenous across the pair of walls with tabs than across the pair of smooth walls.

Turbulent Vortical Structures

The iso-surfaces of the Q-criterion are depicted in Figure 11 to illustrate the coherent vortical structures. The definition of Q follows $Q = \frac{1}{2}(\mathbf{\Omega}^2 - \mathbf{S}^2)$, where $\mathbf{\Omega}$ and $\mathbf{S}$ are the absolute value of vorticity and strain rate, respectively ($\mathbf{\Omega} = \sqrt{2\bar{\omega}_{ij}\bar{\omega}_{ij}}$, $\mathbf{S} = \sqrt{2\bar{S}_{ij}\bar{S}_{ij}}$). Positive Q iso-surfaces isolate areas where the strength of rotation overcomes the strain, thus making those surfaces eligible

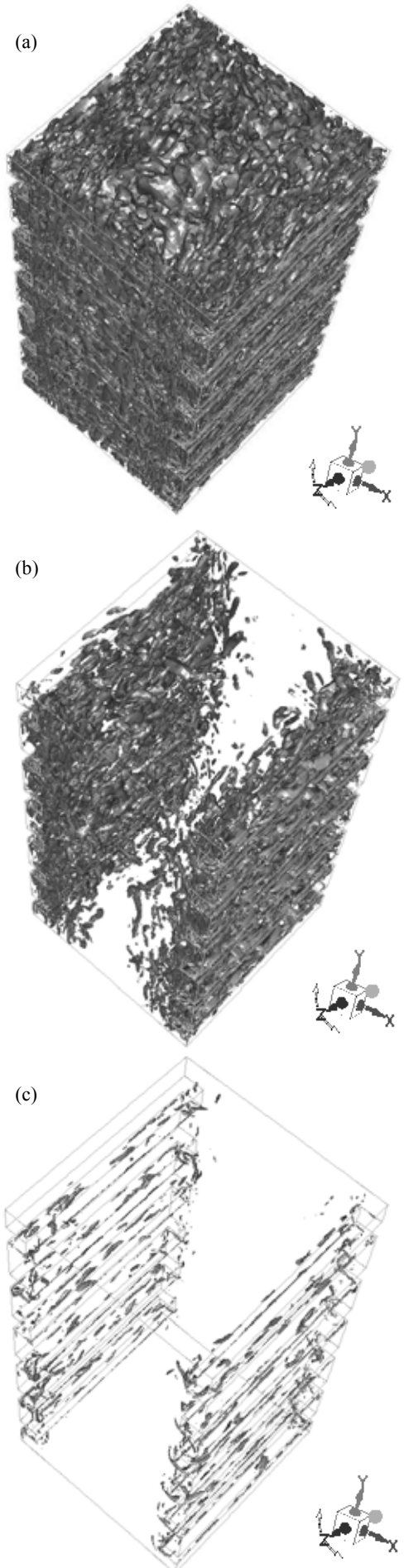

Figure 11: Iso-surfaces of the Q-criterion ($\bar{V} = 2m/s$). (a) Q=10^4; (b) Q=10^6; (c) Q=10^7.

as vortex envelopes (Dubief and Delcayre, 2000; Jeong and Hussain,1995). The dimensional Q-values can be very large and can vary greatly in the domain. For the case under consideration, the Q-values between 10^{-9} and 10^{9}. Iso-surfaces in the range of 10^{4}~10^{7} are sensible to illustrate the turbulent vortical structures for this case. Figures 11 (a) to (c) illustrate the iso-surfaces of Q values of 10^{4}, 10^{6}, and 10^{7}, respectively. It is demonstrated that there are more coherent strong vortices in the region close to the wall with tabs. Tip vortices are produced around the corners behind the tabs (see Figure 11 (c)). One basic question on droplet breakage is whether vortices smaller or larger than the droplets control the breakup rate. Earlier studies assumed that only eddies smaller than the particle diameter may transmit the energy to particles. More recent studies concluded that all scales of turbulent vortices affect the breakup (see for example, Andersson and Helmi, 2014; Ghasempour et al. 2014; Solsvik and Jakobsen, 2016a and 2016b; Solsvik, 2017). When experimental results on the probability of droplet breakage positions are obtained in the future, this information would be further used to provide some insight into the breakage mechanism.

CONCLUSIONS

In this study, an experimental apparatus for investigating single droplet breakage in turbulent flow has been presented as well as some preliminary experimental results. CFD simulation of the single-phase flow in the experimental breakage channel was performed. The LES method was used for the simulation to provide detailed features of the flow. Results from LES were also compared with those from a RANS model (SST k-ω); different degrees of variance were shown in the profiles of velocity, turbulent kinetic energy, and the turbulent energy dissipation rate. The simulation results demonstrated that the turbulence level is enhanced across the pair of walls with protuberances/tabs. There are more coherent strong vortices in the region close to the wall with tabs. Systematic experimental tests will be carried out in the future to obtain statistical information on droplet breakage. The breakage mechanism will be investigated by analysing the experimental results together with the underlying turbulent information obtained from the present numerical study.

ACKNOWLEDGEMENT

This work was carried out as a part of SUBPRO, a Research-based Innovation Centre within Subsea Production and Processing. The authors gratefully acknowledge the financial support from SUBPRO, which is financed by the Research Council of Norway, major industry partners and NTNU. Also, the authors would like to acknowledge the computational resources at NTNU provided by NOTUR, with which the CFD simulations were conducted.

REFERENCES

Andersson, R. and Andersson, B. (2006) On the breakup of fluid particles in turbulent flows. *AIChE journal, 52*(6), pp. 2020-2030.

Andersson, R. and Helmi, A. (2014) Computational fluid dynamics simulation of fluid particle fragmentation in turbulent flows. *Applied Mathematical Modelling, 38*(17), pp. 4186-4196.

Angeli, P. and Hewitt, G. F. (2000) Drop size distributions in horizontal oil-water dispersed flows. *Chemical Engineering Science, 55*(16), pp. 3133-3143.

Azizi, F. and Al Taweel, A. (2011) Turbulently flowing liquid–liquid dispersions. Part I: drop breakage and coalescence. *Chemical Engineering Journal, 166*(2), pp. 715-725.

Bouaifi, M., Mortensen, M., Andersson, R., Orciuch, W., Andersson, B., Chopard, F. and Noren, T. (2004) Experimental and numerical investigations of a jet mixing in a multifunctional channel reactor: Passive and reactive systems. *Chemical Engineering Research and Design, 82*(2), pp. 274-283.

Calabrese, R., Wang, C. and Bryner, N. (1986) Drop breakup in turbulent stirred-tank contactors. Part III: Correlations for mean size and drop size distribution. *AIChE journal, 32*(4), pp. 677-681.

Coulaloglou, C. and Tavlarides, L. (1976) Drop size distributions and coalescence frequencies of liquid-liquid dispersions in flow vessels. *AIChE journal, 22*(2), pp. 289-297.

de Jong, J., Cao, L., Woodward, S., Salazar, J., Collins, L. and Meng, H. (2009) Dissipation rate estimation from PIV in zero-mean isotropic turbulence. *Experiments in fluids, 46*(3), pp. 499-515.

Delafosse, A., Collignon, M.-L., Crine, M. and Toye, D. (2011) Estimation of the turbulent kinetic energy dissipation rate from 2D-PIV measurements in a vessel stirred by an axial Mixel TTP impeller. *Chemical Engineering Science, 66*(8), pp. 1728-1737.

Dubief, Y. and Delcayre, F. (2000) On coherent-vortex identification in turbulence. *Journal of turbulence, 1*(1), pp. 011-011.

Ghasempour, F., Andersson, R., Andersson, B. and Bergstrom, D. J. (2014) Number density of turbulent vortices in the entire energy spectrum. AIChE journal, 60(11), pp. 3989-3995.

Jeong, J. and Hussain, F. (1995) On the identification of a vortex. *Journal of Fluid Mechanics, 285*, pp. 69-94.

Lasheras, J. C., Eastwood, C., Martínez-Bazán, C. and Montañés, J. (2002) A review of statistical models for the break-up of an immiscible fluid immersed into a fully developed turbulent flow. *International Journal of Multiphase Flow, 28*(2), pp. 247-278.

Liao, Y. and Lucas, D. (2009) A literature review of theoretical models for drop and bubble breakup in turbulent dispersions. *Chemical Engineering Science, 64*(15), pp. 3389-3406.

Maaß, S., Gäbler, A., Zaccone, A., Paschedag, A. and Kraume, M. (2007) Experimental investigations and modelling of breakage phenomena in stirred liquid/liquid systems. *Chemical Engineering Research and Design, 85*(5), pp. 703-709.

Maaß, S. and Kraume, M. (2012) Determination of breakage rates using single drop experiments. *Chemical Engineering Science, 70*, pp. 146-164.

Middleman, S. (1974) Drop size distributions produced by turbulent pipe flow of immiscible fluids through a static mixer. *Industrial & Engineering Chemistry Process Design and Development, 13*(1), pp. 78-83.

Ni, X., Jian, H. and Fitch, A. (2003) Evaluation of turbulent integral length scale in an oscillatory baffled

column using large eddy simulation and digital particle image velocimetry. *Chemical Engineering Research and Design, 81*(8), pp. 842-853.

Sheng, J., Meng, H. and Fox, R. (2000) A large eddy PIV method for turbulence dissipation rate estimation. *Chemical Engineering Science, 55*(20), pp. 4423-4434.

Sleicher, C. (1962) Maximum stable drop size in turbulent flow. *AIChE journal, 8*(4), pp. 471-477.

Solsvik, J. and Jakobsen, H. A. (2015) Single drop breakup experiments in stirred liquid–liquid tank. *Chemical Engineering Science, 131*, pp. 219-234.

Solsvik, J., Tangen, S. and Jakobsen, H. A. (2013) On the constitutive equations for fluid particle breakage. *Reviews in Chemical Engineering, 29*(5), pp. 241-356.

Sprow, F. (1967) Distribution of drop sizes produced in turbulent liquid-liquid dispersion. *Chemical Engineering Science, 22*(3), pp. 435-442.

Wang, C. and Calabrese, R. V. (1986) Drop breakup in turbulent stirred-tank contactors. Part II: Relative influence of viscosity and interfacial tension. *AIChE journal, 32*(4), pp. 667-676.

Wilcox, D. C. (1998) *Turbulence modeling for CFD,* California: DCW industries